# Ecdysoneless Overexpression Drives Mammary Tumorigenesis through Upregulation of C-MYC and Glucose Metabolism

Bhopal C. Mohapatra[1], Sameer Mirza[1], Aditya Bele[1], Channabasavaiah B. Gurumurthy[1], Mohsin Raza[1], Irfana Saleem[2], Matthew D. Storck[3], Aniruddha Sarkar[1], Sai Sundeep Kollala[3], Surendra K. Shukla[3], Siddesh Southekal[1], Kay-Uwe Wagner[3], Fang Qiu[4], Subodh M. Lele[5,6], Mansour A. Alsaleem[7,8], Emad A. Rakha[7], Chittibabu Guda[6], Pankaj K. Singh[1,2,3,6], Robert D. Cardiff[9], Hamid Band[1,2,3,5,6], and Vimla Band[1,2,6]

## ABSTRACT

Ecdysoneless (ECD) protein is essential for embryogenesis, cell-cycle progression, and cellular stress mitigation with an emerging role in mRNA biogenesis. We have previously shown that ECD protein as well as its mRNA are overexpressed in breast cancer and ECD overexpression predicts shorter survival in patients with breast cancer. However, the genetic evidence for an oncogenic role of ECD has not been established. Here, we generated transgenic mice with mammary epithelium-targeted overexpression of an inducible human *ECD* transgene (*ECD*Tg). Significantly, *ECD*Tg mice develop mammary hyperplasia, preneoplastic lesions, and heterogeneous tumors with occasional lung metastasis. *ECD*Tg tumors exhibit epithelial to mesenchymal transition and cancer stem cell characteristics. Organoid cultures of *ECD*Tg tumors showed ECD dependency for *in vitro* oncogenic phenotype and *in vivo* growth when implanted in mice. RNA sequencing (RNA-seq) analysis of *ECD*Tg tumors showed a c-MYC signature, and alterations in ECD levels regulated c-MYC mRNA and protein levels as well as glucose metabolism. ECD knockdown-induced decrease in glucose uptake was rescued by overexpression of mouse ECD as well as c-MYC. Publicly available expression data analyses showed a significant correlation of *ECD* and *c-MYC* overexpression in breast cancer, and *ECD* and *c-MYC* coexpression exhibits worse survival in patients with breast cancer. Taken together, we establish a novel role of overexpressed ECD as an oncogenesis driver in the mouse mammary gland through upregulation of c-MYC–mediated glucose metabolism.

**Implications:** We demonstrate ECD overexpression in the mammary gland of mice led to the development of a tumor progression model through upregulation of c-MYC signaling and glucose metabolism.

## Introduction

The mammalian Ecdysoneless (ECD) is the highly conserved orthologue of Drosophila ecdysoneless (*Ecd*) whose mutations lead to developmental arrest (1). *Ecd* interacts with the spliceosome component pre-mRNA processing 8 (Prp8; ref. 2), and loss of Prp8 or *Ecd* led to defective splicing (3). ECD associates with several RNA biogenesis components such as DDX39A and regulates nuclear mRNA export (4), as well as mRNA splicing machinery to regulate mRNA splicing (5).

While the structure of ECD has not been determined, small angle X-ray scattering analyses showed that the first 400 residues of ECD are globular and the next 100 residues exhibit an extended cylindrical structure (6). Others and we have shown that ECD interacts with PIH1D1 and RUVBL1 components of the **p**article for **a**rrangement of **q**uaternary structure (PAQosome), a novel multi-subunit cochaperone complex (7, 8). Notably, ECD, PRPF8, and R2TP subunits are present in a single multi-protein complex (8, 9).

[1]Department of Genetics, Cell Biology and Anatomy, College of Medicine, University of Nebraska Medical Center, Omaha, Nebraska. [2]Department of Biochemistry and Molecular Biology, College of Medicine, University of Nebraska Medical Center, Omaha, Nebraska. [3]Eppley Institute for Research in Cancer and Allied Diseases, University of Nebraska Medical Center, Omaha, Nebraska. [4]Department of Biostatistics, College of Public Health, University of Nebraska Medical Center, Omaha, Nebraska. [5]Pathology and Microbiology, College of Medicine, University of Nebraska Medical Center, Omaha, Nebraska. [6]Fred & Pamela Buffett Cancer Center, University of Nebraska Medical Center, Omaha, Nebraska. [7]Department of Pathology, School of Medicine, University of Nottingham, Nottingham, United Kingdom. [8]Department of Applied Medical Sciences, Applied College, Qassim University, Qassim, Saudi Arabia. [9]Department of Pathology and Laboratory Medicine, University of California, Davis, California.

Current address for C.B.Gurumurthy: Mouse Genome Engineering Core Facility, Department of Pharmacology and Experimental Neuroscience, University of Nebraska Medical Center, Omaha, Nebraska; current address for K.-U. Wagner, Department of Oncology, Karmanos Cancer Institute, Wayne State University School of Medicine, Detroit, Michigan; current address for S.K.Shukla and P.K. Singh, Department of Oncology Science, University of Oklahoma Health Sciences Center, Oklahoma City, Oklahoma.

B.C. Mohapatra and S. Mirza contributed equally to this article.

**Corresponding Authors:** Vimla Band, Department of Genetics Cell Biology & Anatomy, University of Nebraska Medical Center, 985805 Nebraska Medical Center, Omaha, NE, 68198. Phone: 402–559–8565; E-mail: vband@unmc.edu; and Hamid Band, Eppley Institute for Research in Cancer and Allied Disease, 985950 Nebraska Medical Center, Omaha, NE 68198-5950. Phone: 402–559–8572; E-mail: hband@unmc.edu

Mol Cancer Res 2022;20:1391–404

**doi:** 10.1158/1541-7786.MCR-22-0122

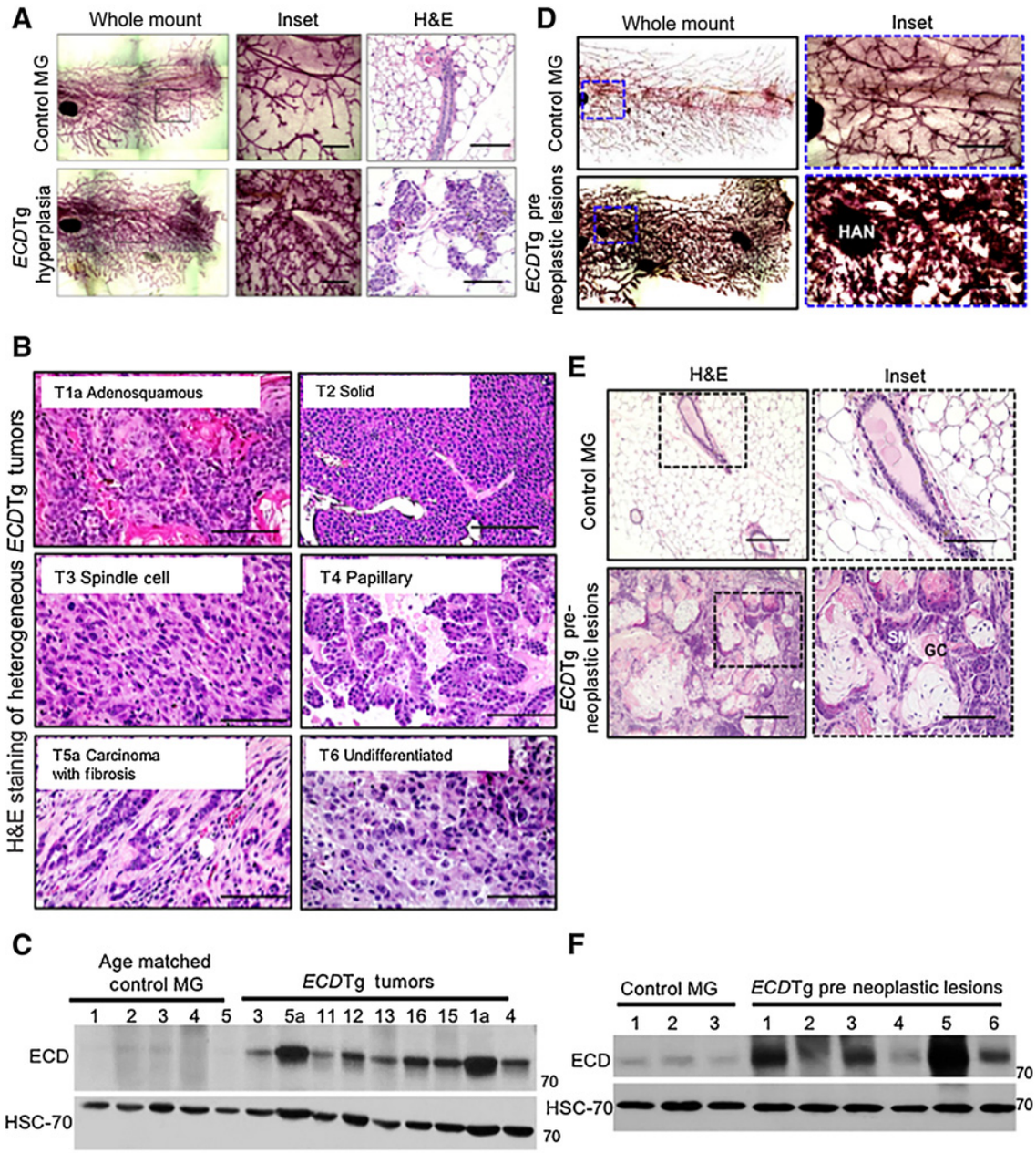


**Figure 1.**

ECD overexpression promotes mammary gland hyperplasia, heterogeneous tumors, and preneoplastic lesions. **A,** Representative whole-mount staining images of littermate control and mouse mammary gland in *ECD*Tg mouse at 5 to 6 months of age. Scale bar, 400 μm; inset 1,000 μm. **B,** H&E staining of *ECD*Tg tumors. Scale bar, 100 μm. **C,** Western blot for ECD expression (tumor numbers in Supplementary Table S1). **D,** Age-matched control and *ECD*Tg mammary gland at 15 to 25 months, inset 1,000 μm. **E,** H&E staining of *ECD*Tg mammary gland. Scale bar, 400 μm; and inset 100 μm. **F,** Western blot for ECD protein. HSC-70, used as a loading control. MG, mammary gland.

We showed that germline deletion of *ECD* in mice leads to embryonic lethality and deletion of *ECD* in cells led to cell cycle arrest (10). We showed a role of ECD in mitigating endoplasmic reticulum (ER) stress (11). ECD also regulates p53 stability, either directly (12) or through TXNIP (13), suggesting a role in genotoxic stress response.

ECD overexpression is frequent in several cancers, such as breast (4, 14), pancreas (15), cervical, head and neck (5), and gastric (16). ECD mRNA and protein overexpression in patients with breast cancer correlate with shorter survival (4, 14). Overexpressed ECD cooperates with mutant Ras to transform immortal human mammary epithelial cells (hMEC; ref. 17), as well as ECD

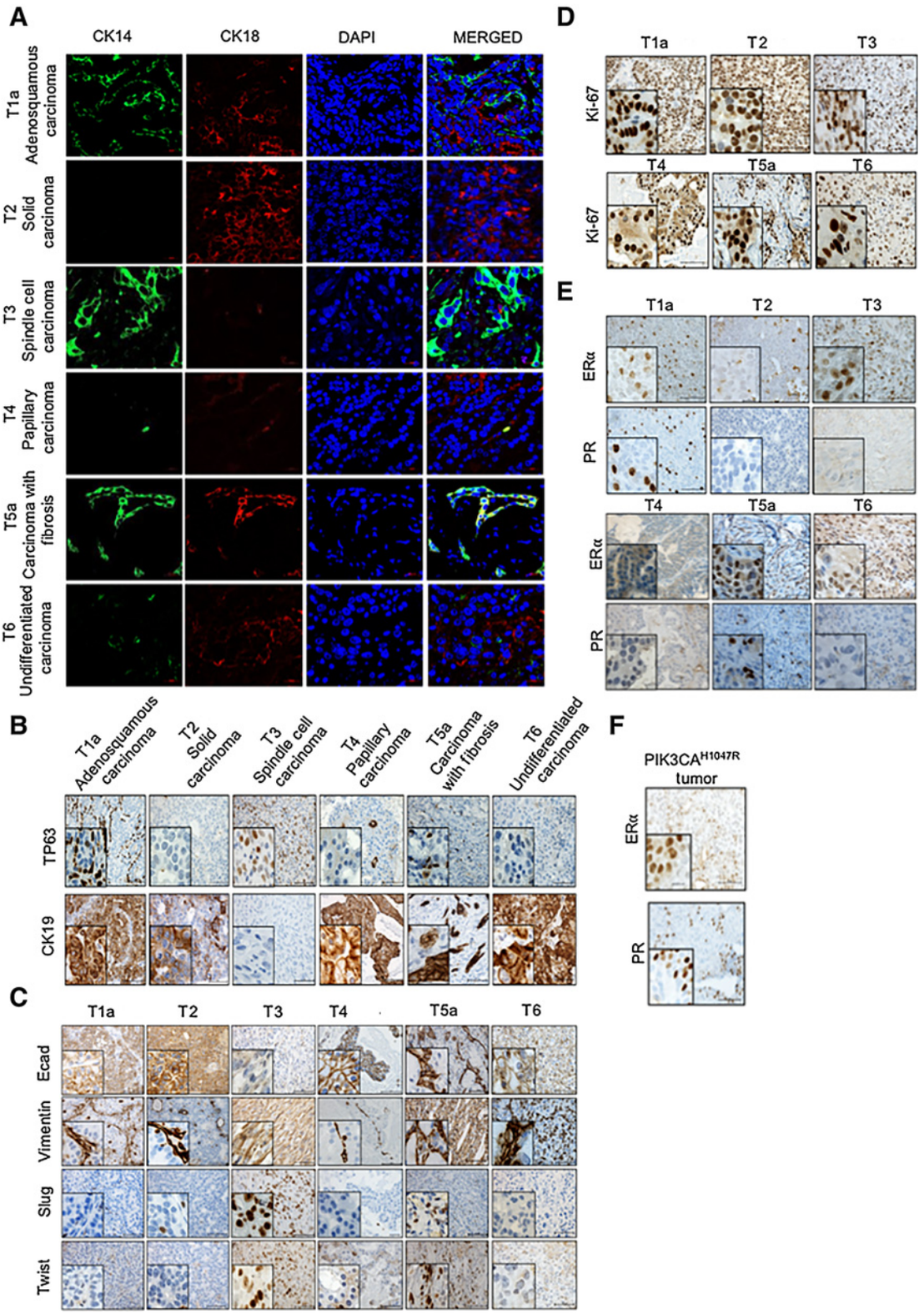


**Figure 2.**

Characterization of *ECD*Tg tumors by IHC. **A–F,** *ECD*Tg tumor subtypes were immunostained with indicated antibodies. Scale bar, 50 μm (magnification 400×); inset scale bar, 10 μm (magnification 1,000×).

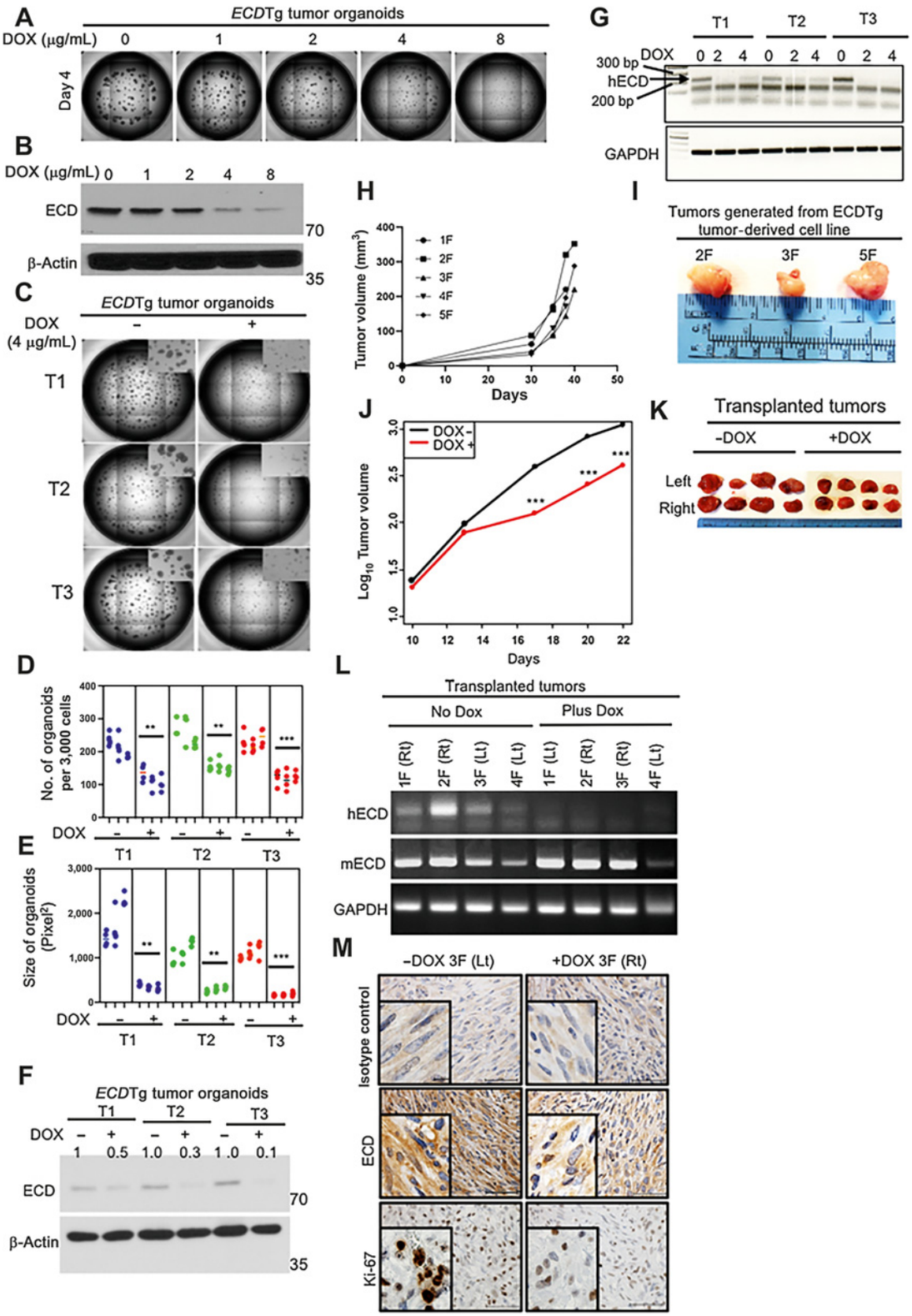

cooperates with human papillomavirus (HPV)16 E7 to immortalize keratinocytes (5).

Given the evidence for a prooncogenic role of ECD, here we generated *ECD* transgenic mice [Tet(O)-ECD; MMTV-tTA, hereafter called *ECD* transgene *(ECD*Tg) mice] to target *ECD* overexpression in the mouse mammary epithelium. Notably, *ECD*Tg mice led to mammary hyperplasia followed by preneoplastic lesions or heterogenous tumors with aging. The *ECD*Tg mice tumors exhibited epithelial to mesenchymal transition (EMT) and ECD dependency for *in vitro* organoid growth as well as *in vivo* tumorigenesis upon implantation in mice. *ECD*Tg overexpression upregulates *c-MYC* mRNA and protein expression by regulating *c-MYC* mRNA as well as protein stability, and consequently affecting glucose metabolism. These findings support a prooncogenic role of ECD overexpression in breast cancer through upregulation of c-MYC and glucose metabolism.

## Materials and Methods

Detailed Materials and Methods of the following sections are included in Supplementary Information: antibodies, media, reagents, chemicals and cell culture, generation of Tet(O)-*ECD* transgenic mouse, mammary gland harvest and whole-mount staining, tumor organoid growth and analysis, tumor transplantation, immunohistochemistry (IHC), Western blotting, RNA isolation and real time-PCR analysis, transcriptome analysis by RNA sequencing (RNA-seq) analysis, RNA stability, metabolites extraction and mass spectrometric metabolomics analyses, glucose uptake, METABRIC and KM Plotter database analyses, and statistical analyses.

### Tumor transplantation

*ECD*Tg tumor fragments (~2 $mm^3$) were placed in the cleared mammary fat pads of recipient mice on both sides. At day 10 posttransplantation, palpable tumors were measured, and mice were randomly assorted into two groups: with or without doxycycline + sucrose in drinking water. For other experiments, $2 \times 10^6$ *ECD*Tg tumor-derived cells were injected orthotopically into fourth inguinal mammary gland and tumor growth was monitored over time.

### Metabolites extraction and mass spectrometric metabolomics analyses and glucose uptake

Doxycycline-inducible ECD overexpressing (ECD-OE) MCF10A and 76NTERT cells were cultured with or without doxycycline for 72 hours and were subjected to metabolomics analyses as described previously (18). Similarly, *ECD*Tg tumor organoids grown as suspension in presence and absence of doxycycline for 96 hours were processed for metabolomics. Glucose uptake assay was performed in following cells *ECD*Tg organoids (±doxycycline), doxycycline-inducible ECD-overexpression (OE; +doxycycline) and controls (-doxycycline) MCF10A and 76NTERT cells and control and ECD knockdown (KD) SUM-159 cells as described previously (4). The detailed procedures are included in Supplementary Information.

### Human and animal subjects

Mice uses in this study were preapproved by the University of Nebraska Medical Center Institutional Animal Care and Use Committee (IACUC) and is in compliance with Federal and State guidelines

## Results

### ECD overexpression promotes mammary hyperplasia, preneoplastic mammary gland lesions, and tumor formation

To directly assess the role of ECD in oncogenesis, we generated transgenic mice with germline incorporation of a Tet(O)-Flag-*ECD*-IRES-eGFP construct, designed to regulate human *ECD* gene overexpression in the mouse mammary gland under doxycycline control (Supplementary Fig. S1A). Further crossing of these mice with transgenic mice bearing an MMTV-tTA transgene (19) resulted in Tet(O)-Flag-*ECD*-IRES-eGFP; MMTV-tTA double-transgenic mice (designated as *ECD*Tg; Supplementary Fig. S1B).

Comparison of the mammary glands of 5 to 6 months old *ECD*Tg mice with single transgene-expressing age-matched littermate controls showed increased ductal branching and lobulo-alveolar development (**Fig. 1A**; Supplementary Fig. S2A) as seen with other mammary transgenic models (20, 21). Overall, 85% (6 of 7 examined) *ECD*Tg mice exhibited mammary gland hyperplasia compared with none (0 of 7 mice) in control mice. Hyperplasia showed overexpression of ECD protein and smooth muscle myosin (Supplementary Fig. S2B), a marker of hyperplasia (22).

Notably, 33% (17 of 51) of *ECD*Tg mice exhibited heterogeneous tumors by 15 to 25 months of age, and 1 of these 17 mice showed lung metastasis (**Fig. 1B**; Supplementary Table S1), which was positive for ECD and CK14, patchy CK19 staining, and was negative for the Clara cells marker CC10 (Supplementary Fig. S3). *ECD*Tg tumors were heterogeneous with distinct histologic subtypes (**Fig. 1B**), as is the case with other genetically engineered mouse models of breast cancer, such as *C-MYC* and *WNT* (23). Of 17 tumors, 7 were of the adenosquamous type and 4 tumors exhibited spindle cell morphology with EMT characteristics, 2 tumors showed solid carcinoma morphology characterized by epithelial cells arranged in sheet-like structures, 2 tumors were papillary type characterized by projections of epithelial cells, 1 showed carcinoma with fibrosis, and 1 tumor was partially necrotic with undifferentiated histology. As anti-ECD antibodies cross-react with human and mouse ECD, use of human ECD specific primers showed expected human *ECD* mRNA in *ECD*Tg tumors (few examples shown in Supplementary Fig. S2C). *ECD*Tg tumors showed expected higher expression of ECD protein (**Fig. 1C**), and IHC analysis confirmed ECD staining (Supplementary Fig. S2D).



**Figure 3.**

Organoid formation and tumor growth of *ECD*Tg tumor-derived cells. **A,** Images of organoids upon doxycycline treatment. **B,** Western blot of lysates from organoids, β-actin used as a loading control. **C,** Three independent tumors ±doxycycline, insets show high magnification. Scale bar, 400 μm. **D** and **E,** Organoid number and size after 4 days of doxycycline treatment ($N = 3$ times and 4 wells per condition). **, $P < 0.01$; ***, $P < 0.001$. Data represents mean ± SEM with two tailed unpaired *t* test, and nested *t* test. **F,** Western blot shows ECD expression; densitometry in respect to without doxycycline in each tumor normalized with β-actin, shown below. **G,** qRT-PCR using human *ECD* specific primers. **H,** T3 organoids were injected orthotopically into 5 NSG mice. The tumor growth is plotted as tumor volume over days. **I,** Images of the isolated tumors. 2 of the mice (1F and 4F) died during experiment due to unknown reason. **J,** tumor fragments of 2 $mm^3$ size from T3 were transplanted in NSG mice. After 10 days, the tumor volume was measured and mice were distributed into two groups for with and without doxycycline treatment, and growth was monitored for the next 12 days. Mean ± SEM of tumors is calculated by mixed model of ANOVA analysis. ***, $P < 0.001$. **K,** Images of the tumors harvested after the dissection. **L,** qRT-PCR using human and mouse ECD specific primers. **M,** IHC of tumor sections from doxycycline-treated mice 3F, stained with indicated antibodies. DOX, doxycycline. Lt, left; Rt, right.

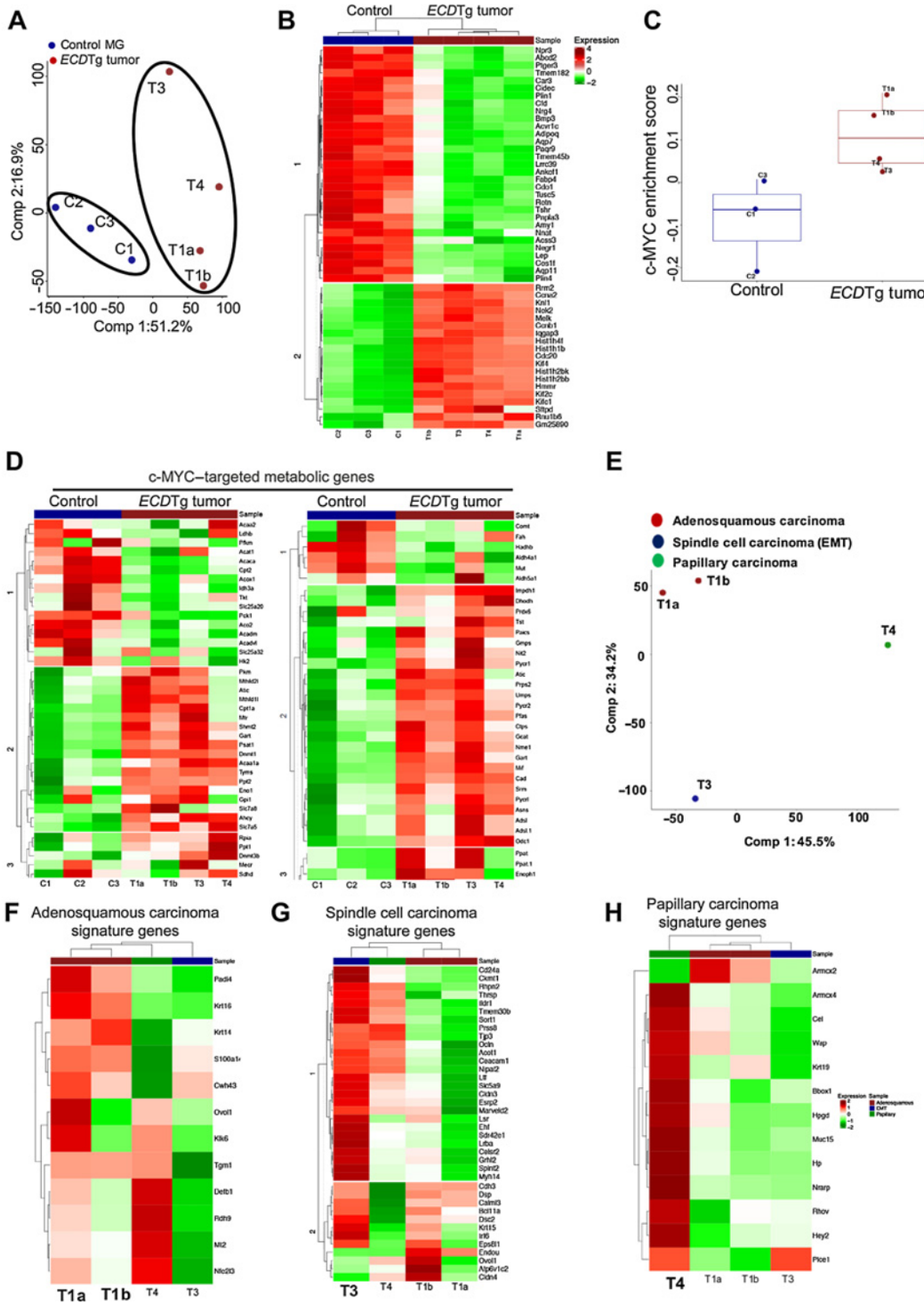


**Figure 4.**

RNA-seq analyses comparison of *ECD*Tg tumors and control mammary glands. **A,** Principal component analysis (PCA) analysis of RNA-seq data shows clustering of control mammary glands and *ECD*Tg tumor datasets. First Principal component (PC1), 51.2% viability; and Second Principal component (PC2), 16.9% viability. **B,** Heatmap of the top 50 differentially expressed genes among different biologic replicates of control mammary glands and tumors. Upregulated genes in red, downregulated genes in green. **C,** Box plot shows the enrichment scores obtained using single sample Gene Set Enrichment Analysis of the c-MYC signature genes. **D,** MYC-regulated metabolic genes in *ECD*Tg tumors. RNA-seq followed by cluster comparison analyses of 4 tumors. 82 up- and downregulated genes are shown. Red (upregulated) green (downregulated). **E,** PCA shows clustering of *ECD*Tg tumors ($n = 4$) based on tumor type. PC1 represent 45.5% viability and PC2 represent 34.2% viability. **F,** Heatmap shows heterogeneity among the tumors. **G,** Heatmap depicting EMT signature upregulated in spindle cell carcinoma (Tumor#T3). **H,** Heatmap displaying papillary carcinoma signature genes upregulation in papillary carcinoma (T4).

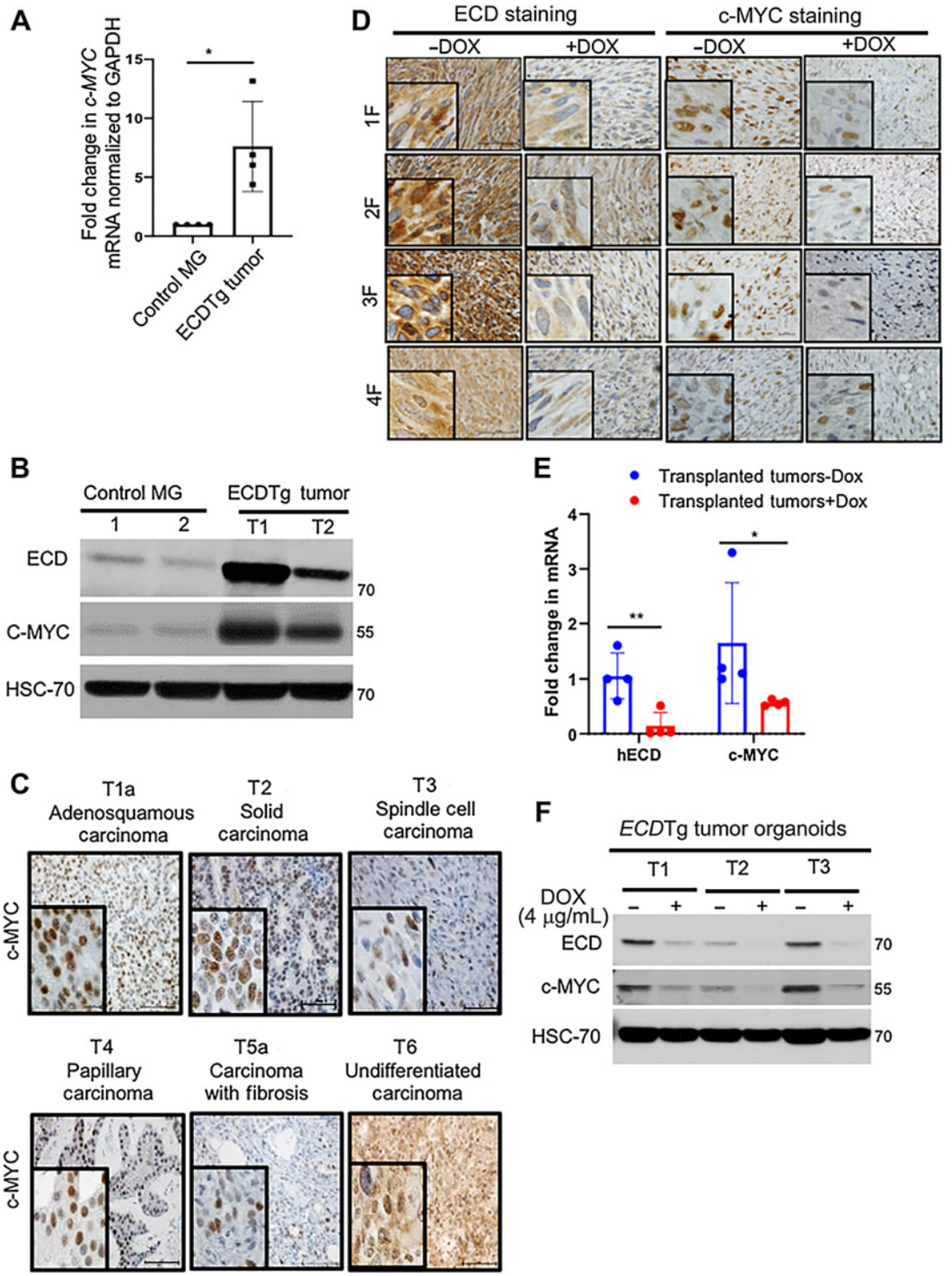


**Figure 5.**

*ECD*Tg tumors exhibit upregulation of c-MYC. **A,** qRT-PCR shows increased *c-Myc*, mRNA in tumors. Bar graph shows fold change of mRNAs (controls, $n = 4$; and tumors, $n = 4$). *, $P < 0.05$. **B,** Western blot with indicated antibodies. HSC-70, used as a loading control. **C,** IHC of indicated tumors and c-MYC staining. **D** and **E,** Representative IHC images and qRT-PCR mRNA expression analysis of 4 independent *ECD*Tg transplanted tumors from doxycycline-untreated or doxycycline-treated mice. **F,** Western blot of lysates of organoids. HSC-70 used as a loading control. DOX, doxycycline.

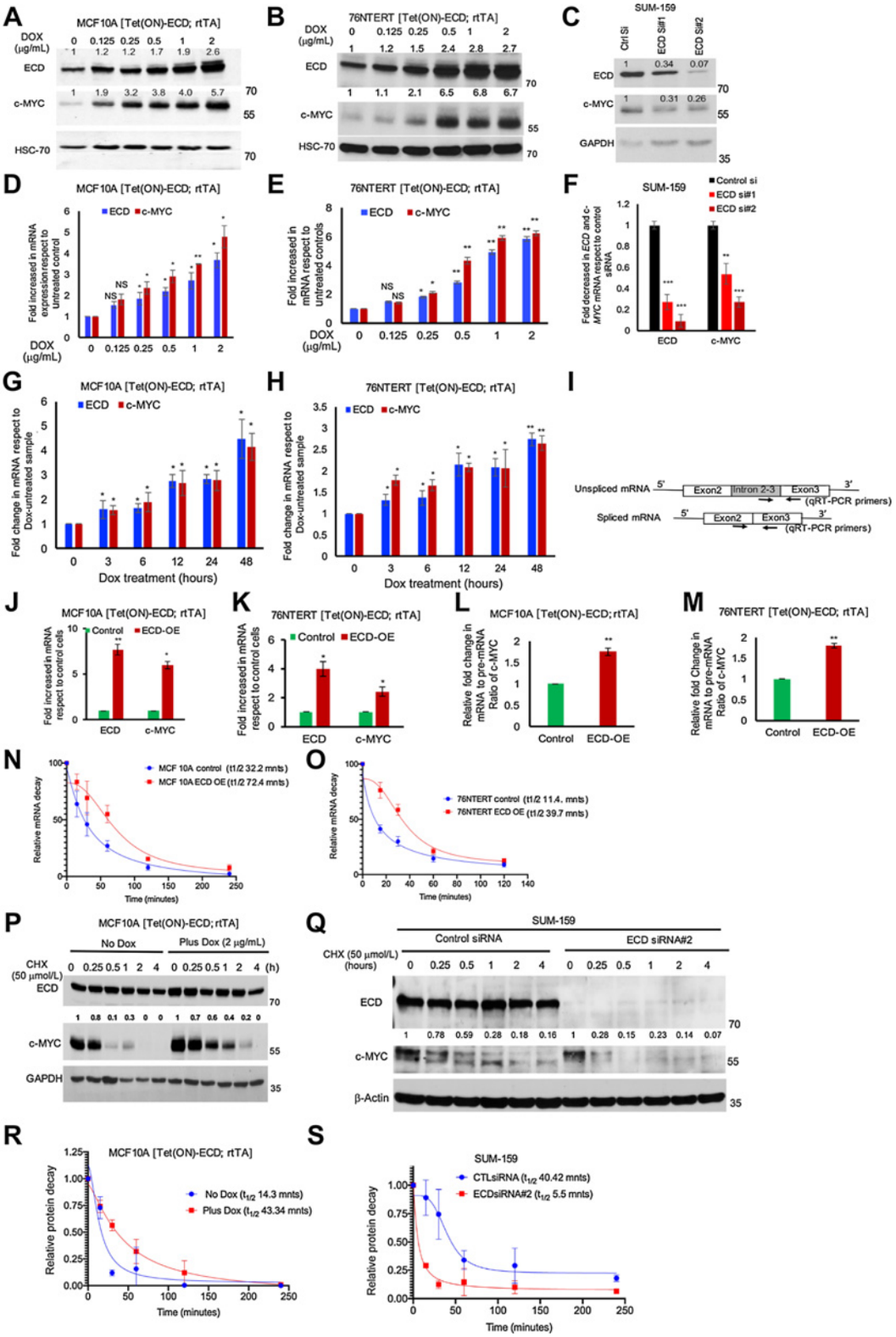

Histologic analysis of the remaining 34 tumor-free *ECD*Tg mice revealed that 29 (85%; 57% of the overall *ECD*Tg cohort) of these mice exhibited abnormal mammary gland histology with distended hyperplastic alveolar nodules and lipid accumulation in the ducts and lobules (Supplementary Table S2; **Fig. 1D**). Hematoxylin and eosin (H&E) staining showed squamous metaplasia, atypical nuclei, glandular differentiation, a dense stroma, lymphocytic infiltration, and dark proteinaceous staining inside alveolar lumen (**Fig. 1E**) similar to other transgenic models (24), with higher levels of ECD protein (**Fig. 1F**). In comparison with the *ECD*Tg mice, only 4 of 17 (23.5%) age-matched control mice exhibited some squamous nodules with ductal ectasia, distinct morphology from *ECD*Tg mice derived lesions (Supplementary Table S2) as seen in other transgenic models (25, 26). Of the 34 *ECD*Tg mice analyzed, 9 of 11 were parous mice and 20 of 23 were nulliparous mice that developed neoplasia, whereas only 4 of 15 nulliparous and none of 2 parous age-matched control mice had abnormal mammary glands.

IHC showed strong positive cytokeratin (CK)14 expression in adenosquamous tumor, spindle cell carcinoma, and carcinoma with fibrosis (**Fig. 2A**). Positive CK18 staining was seen in adenosquamous carcinoma, solid carcinoma, and carcinoma with fibrosis. The undifferentiated carcinoma showed only weak staining for both CK14 and CK18. Several tumors exhibited cells with dual CK14 and CK18 staining, suggestive of the presence of progenitor cells in these tumors (**Fig. 2A** merged image; ref. 27). Furthermore, nuclear p63, basal mammary epithelial cell marker (21) and CK19, glandular epithelial cell marker (28) staining was observed in tumors positive for CK14; however, undifferentiated carcinoma type tumors were negative for p63. CK19, a known marker of papillary carcinoma (21, 29) showed strong staining in the papillary carcinoma and adenosquamous carcinoma, and patchy staining in solid carcinoma, carcinoma with fibrosis and undifferentiated carcinoma. However, spindle cell carcinoma was negative for CK19 (**Fig. 2B**).

About 26% of *ECD*Tg tumors displayed the EMT phenotype, spindle cell carcinoma showed lack of E-cadherin and upregulation of vimentin, slug, and twist; however, carcinoma with fibrosis was positive for E-cadherin and showed upregulation of vimentin, slug, and twist (**Fig. 2C**) similar to other transgenic models (30, 31). The remaining histologic subtypes of *ECD*Tg tumors showed E-cadherin staining. Vimentin staining in the fibrous parts of tumors was observed in all subtypes (**Fig. 2C**). *ECD*Tg tumors were highly positive for Ki-67, irrespective of the subtypes (**Fig. 2D**).

A subset of reported genetically engineered mouse model (GEMM) tumors are estrogen receptor positive ($ER^+$), such as cyclin D1 or PIK3CA (32, 33). Our analysis revealed that 7 of 17 (41%) *ECD*Tg tumors were $ER^+$, with 2 tumors positive for both ER and progesterone receptor (PR; **Fig. 2E**). Our results are consistent with reported transgenic models of $Met^{mut}$, retinoblastoma protein (RB) deletion (27, 34), and MMTV-$PIK3CA^{H1047R}$ (35). Tumors from PIK3CA mice were used as positive control in our experiment (**Fig. 2F**).

## ECD overexpression is required for the maintenance of tumorigenic phenotype of *ECD*Tg tumors

Next, we established and characterized organoid cultures *of ECD*Tg tumors. Notably, doxycycline dose-dependent decrease in the levels of ECD protein correlated with organoid forming efficiency (**Fig. 3A** and **B**), organoid number, and sizes (**Fig. 3C–E**). Expected doxycycline-dependent decrease in ECD protein as well as human ECD mRNA were observed (**Fig. 3F** and **G**). The long latency and low penetrance precluded analyses using *in vivo* doxycycline-inducible attenuation of the transgenic ECD expression. Therefore, *ECD*Tg tumor organoid-derived cells were orthotopically injected into the mammary fat pads of athymic nude mice, similar to the literature (36). Easily palpable tumors were observed within 1 month of injections, and these tumors grew rapidly afterward (**Fig. 3H** and **I**). In addition, similar to the literature (37) transplantation of *ECD*Tg tumor fragments into NOD/SCID gamma (NSG) mice for 10 days, and then switching 50% mice to doxycycline-containing water with further monitoring tumor growth over 12 days showed a significant reduction in the tumor growth rate and final tumor size in the doxycycline-treated group (**Fig. 3J** and **K**). qRT-PCR analysis of mouse and human ECD mRNA expression using human ECD specific primers showed doxycycline-inducible decrease in human ECD mRNA levels (**Fig. 3L**). IHC analysis confirmed the reduction in ECD expression in tumors from the doxycycline-treated group with a concomitant reduction in Ki-67 staining (**Fig. 3M**). Histologically, the transplanted tumors were comparable with the original tumors (Supplementary Fig. S4).

## RNA-seq analysis of *ECD*Tg tumors reveals heterogeneity and upregulation of MYC target metabolic genes

RNA-seq analysis of 4 *ECD*Tg tumors (2 adenosquamous carcinoma, 1 spindle cell carcinoma, and 1 papillary) in comparison with three control mammary glands of 6-month–old virgin female mice, followed by principal component analysis (PCA) showed distinct clusters corresponding to tumors and control mammary glands (**Fig. 4A**). Differential gene expression (DEG) analysis showed that 2,210 genes were differentially expressed between tumors and controls of which the top 50 are shown as a heatmap (**Fig. 4B**). Notably, several genes associated with the basal subtype of breast cancers (*Trp63, CK14, CK15*, and *CK17)*, cell-cycle regulated genes (*E2F1*, *CENPI*, *Ccnb1*, *Mcm5, cMyc)*, and histone H2B gene family members (*Hist1h2bj, Hist1h2af, Hist1h1e*) were upregulated in tumor samples. Several genes, such as *Abcd2, Cidec, Plin1, Aqp7, Fabp4, Lep*, and *Bmp3* that

**Figure 6.**

c-MYC mRNA levels and protein stability upon alterations in ECD levels. Western blot of ECD and c-MYC protein, HSC-70 used as a loading control (**A**–**C**) and mRNA by qRT-PCR (**D**–**F**) in indicated cell lines. **G** and **H,** Time-dependent mRNA expression of c-MYC upon induction of ECD. mRNA quantitation data represents mean ± SEM with two-tailed unpaired *t* test. $n = 3$; *, $P < 0.05$; **, $P < 0.01$; ***, $P < 0.001$. Schematic display of the qPCR primer pairs (marked arrows) used to measure pre-mRNA and mature mRNA species (**I**). Bar graphs show overexpression of *ECD* resulted in upregulation of *c-MYC* mRNA (**J** and **K**). Pre-mRNA to mRNA ratio in ECD-overexpressing cells is shown in bar graphs as fold change in comparison with controls. 18S was used for normalization (**L** and **M**). The stability of c-MYC mRNA was analyzed in doxycycline-inducible ECD-overexpressing indicated cells in the presence or absence of doxycycline for 72 hours. The cells were treated with actinomycin D (5 μg/mL) for indicated time points and qRT-PCR was performed after RNA isolation. GAPDH was used for normalization. Half-life of c-MYC mRNA in MCF10A (**N**) and 76NTERT (**O**). Data represents mean± SE of three independent experiments. The stability of c-MYC protein was analyzed in doxycycline-inducible ECD-overexpressing MCF10A cells in the presence or absence of doxycycline for 72 hours. The cells were treated with cycloheximide (50 μmol/L) for indicated time points and lysates were collected. **P,** Western blot with indicated antibodies. **P** and **R,** Half-life of c-MYC protein in ECD overexpressing MCF10A cells. **Q** and **S,** c-MYC protein stability was analyzed after 48 hours of treatment of SUM-159 with control or ECD siRNA, followed by cycloheximide (CHX) treatment. **Q,** Western blot shows c-MYC protein in ECD KD cells. **S,** Exponential decay plot shows half-life of c-MYC upon ECD KD. Densitometry of c-MYC after normalizing to their respective loading controls, GAPDH and β-actin in comparison with no CHX treatment are indicated on top in (**P**) and (**Q**). NS, not significant; DOX, doxycycline; h, hours; mnts, minutes.

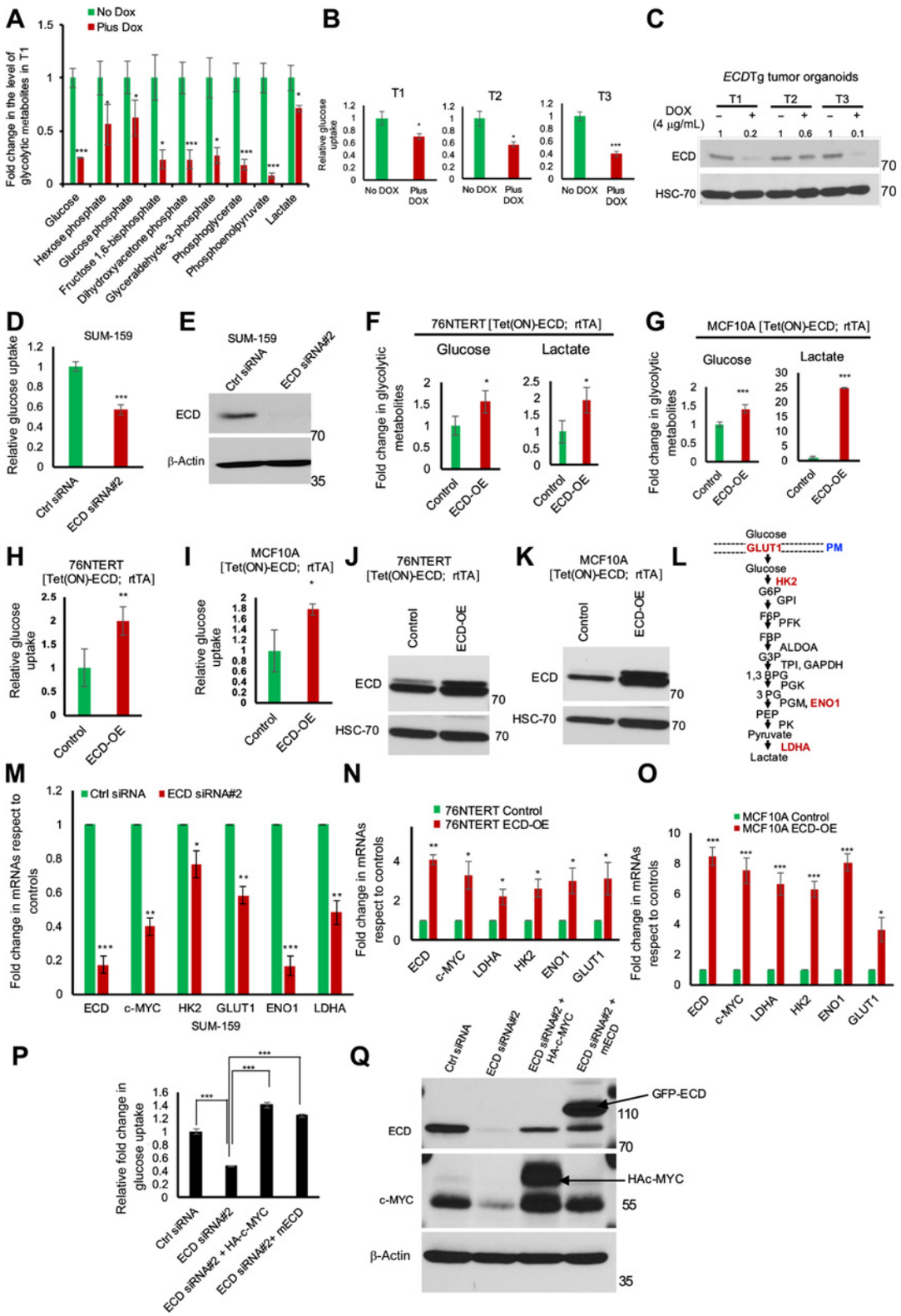

are known to be downregulated in breast cancer (38) were downregulated in *ECD*Tg tumors.

Assessment of the enrichment score using the single-sample gene set enrichment analysis (ssGSEA) method (39), demonstrated enrichment of *c-MYC* signature genes in tumors (**Fig. 4C**), heatmap of 82 up- and downregulated *c-MYC*-regulated genes are shown (**Fig. 4D**). PCA plots identified the individual tumors as belonging to different subtypes as tumor number 3 (T3; spindle cell carcinoma) and tumor number 4 (T4; papillary adenosquamous) were distinct from tumors T1a and T1b (adenosquamous; **Fig. 4E**). We examined the presence of tumor gene signatures associated with the squamous, EMT, and papillary types in our data, based on a public microarray database (21). Notably, upregulation of 12 mRNAs associated with squamous carcinoma signature (T1a and T1b tumors; **Fig. 4F**), 34 upregulated EMT signature genes in the EMT subset (T3; **Fig. 4G**), and upregulation of papillary signature genes (T4; **Fig. 4H**) were seen in *ECD*Tg tumors.

### *ECD*Tg tumors express high *MYC* mRNA and protein

Analysis of tumors and organoids showed *ECD*Tg tumors express high levels of *c-MYC* mRNAs (**Fig. 5A**) as well as c-MYC protein (**Fig. 5B** and **C**). Transplanted tumors showed ECD-dependent regulation of c-MYC upon doxycycline treatment (**Fig. 5D** and **E**). Doxycycline-inducible down regulation of ECD in *ECD*Tg organoids, led to ECD-dependent decrease in c-MYC levels (**Fig. 5F**).

Next, we generated two immortal hMECs, MCF10A and 76NTERT with doxycycline-inducible ECD overexpression. In both cell lines a doxycycline dose-dependent increase in ECD levels led to increase in *c-MYC* mRNA and protein levels (**Fig. 6A**, **B**, **D**, and **E**). Furthermore, siRNA-mediated knockdown of ECD in a breast cancer cell line SUM-159 showed a significant ECD-dependent decrease in c-MYC mRNA and protein levels (**Fig. 6C** and **F**). To demonstrate the effect of ECD on *c-MYC* mRNA is independent of its effect on proliferation, we performed time-dependent doxycycline induction. We observed upregulation of *c-MYC* mRNA as early as 3 hours correlating with ECD mRNA upregulation (**Fig. 6G** and **H**) excluding the proliferation effect of ECD on *c-MYC* mRNA.

Based on our recent work (4, 5) and that of others (2, 3) supporting a role of ECD in splicing of pre-mRNA to mRNA, we assessed the ratio of mRNA over pre-mRNA in control versus ECD overexpressing cells. ECD overexpression increased the ratio of *c-MYC* mRNA to pre-mRNA (**Fig. 6I**–**M**). Next, actinomycin-D treatment of control and doxycycline-inducible ECD overexpressing MCF10A and & 76NTERT cells showed an ECD-dependent increase of *c-MYC* mRNA stability (**Fig. 6N** and **O**). Furthermore, treatment of ECD-overexpressing or ECD KD cells with cycloheximide followed by measurement of protein levels over various time periods showed ECD-dependent increase (in MCF10A) or decrease (in SUM-159) stability of c-MYC protein (**Fig. 6P**–**S**). Taken together, our results demonstrate that ECD regulates stability of both c-MYC mRNA as well as protein.

### ECD regulates the levels of glycolytic metabolites and glucose uptake

RNA-seq analyses of *ECD*Tg tumors showed several c-MYC regulated glucose metabolic genes (**Fig. 4D** and **E**), we thus performed LC-MS/MS–based analysis of metabolites (18) in *ECD*Tg organoids derived from adenosquamous tumor T1 in the presence or absence of doxycycline. These analyses revealed a significant decrease in glycolytic metabolites upon doxycycline treatment (**Fig. 7A**). ECD KD (+doxycycline) in three *ECD*Tg organoids showed a significant decrease in glucose uptake (**Fig. 7B** and **C**) and ECD siRNA KD in a breast cancer cell line showed a decrease in glucose uptake (**Fig. 7D** and **E**). Reciprocally, inducible ECD overexpression showed increased levels of glucose and lactate (**Fig. 7F** and **G**) and increased glucose uptake (**Fig. 7H**–**K**). PCA analysis of ECD-OE (+doxycycline) and control cells (-doxycycline) using top 55 metabolites showed differential metabolic clustering (Supplementary Fig. S5). c-MYC is known to be an important regulator of glycolysis and glycolytic enzymes lactate dehydrogenase A (LDHA), glucose transporter (GLUT1), hexokinase 2 (HK2), and enolase 1 (ENO1; refs. 40, 41). ECD dependent alteration in c-MYC mRNA and c-MYC regulated glycolytic target genes were observed (**Fig. 7L**–**O**).

Finally, decrease in glucose uptake upon ECD siRNA-mediated Knockdown was rescued by mouse ECD (resistant against human ECD specific siRNA) as well as by exogenous c-MYC expression (**Fig. 7P** and **Q**). Taken together, these results demonstrate ECD regulates c-MYC–driven glucose metabolism and thereby glucose uptake.

Consistent with our experimental model, gene correlation analysis was performed to assess the correlation between *ECD* mRNA and *c-MYC* mRNA expression in all patients with breast cancer of the METABRIC cohort ($n = 1{,}980$) and stratified PAM50 molecular subtyped patients with breast cancer (Supplementary Fig. S6A–S6F). Significant correlation of *ECD* and *c-MYC* mRNA expression in all breast cancer and various subtypes of breast cancer was observed (Supplementary Fig. S6A–S6F). Kaplan–Meier plotter (42) and Surveillance Epidemiology and End Results (SEER) prevalence analysis of patients with breast cancer ($n = 493$), split on the basis of trichotomization (T1 vs. T3) with the *ECD* (probe set 202276_at) and *cMYC* mRNA (probe set 202431_s_at) expression for relapse-free survival (RFS) and distant metastasis-free survival (DMFS), showed while *ECD* high versus low ($P = 0.0028$) or *c-MYC* high versus low ($P = 0.038$) expression had statistically significant difference in RFS, combined expression of *ECD* + *c-MYC* high versus *ECD* + *c-MYC* low predicted



**Figure 7.**

Metabolomics analysis of *ECD*Tg tumor cells. **A,** Organoids from *ECD*Tg T1, with or without doxycycline for 4 days, followed by analysis of glycolytic metabolites. Bar diagram shows the fold decrease in the levels of glycolytic metabolites. *, $P < 0.05$; **, $P < 0.01$; ***, $P < 0.001$. **B,** Glucose uptake in three *ECD*Tg tumor organoids (in triplicates). The values were normalized with respective to cell counts and depicted as compared with doxycycline-untreated organoids. Quantification of results from four replicates is shown as a bar graph. *, $P < 0.05$; **, $P < 0.02$; ***, $P < 0.002$. Data represents as mean ± SD and two-tailed unpaired test with Welch correction. **C,** Western blot of lysates from organoids used for experiments in (**A**) and (**B**) HSC-70 used as a loading control. Densitometry of ECD in respect to without doxycycline in each tumor, after normalizing with loading control. **D,** Glucose uptake in control and ECD siRNA-treated cells. **E,** Western blot of ECD protein, β-actin used as a loading control. **F** and **G,** Glycolytic metabolites in hMECs upon doxycycline-inducible ECD upregulation. Bar diagram shows the fold increase in the levels of glucose and lactate in ECD-overexpressing cells compared with control cells. **H** and **I,** Glucose uptake in ECD-overexpressing cells, normalized with respect to cell counts and depicted in comparison with control cells. **J** and **K,** Western blot shows the levels of ECD level in cells used for experiments in (**H**) and (**I**). **L,** Schematic depicts the intermediate products and enzymes of glycolysis. Red-marked are c-MYC–regulated glycolytic enzymes. PM, plasma membrane. mRNA levels of indicated genes in cells upon ECDKD (**M**) or ECD overexpression (**N** and **O**). **P,** Glucose uptake rescue in SUM-159 cells by overexpression of HA-c-MYC or mECD-GFP in ECD KD cells. In each case *, $P < 0.05$; **, $P < 0.01$; ***, $P < 0.001$. Data represents as mean ± SD of four replicates and two-tailed unpaired tests with Welch correction. **Q,** Western blot shows expression of indicated proteins. β-actin used as a loading control. DOX, doxycycline; ctrl, control.

more significant RFS ($P = 0.0013$; Supplementary Fig. S6G). Notably, while DMFS probability of *ECD* high versus low expression ($P = 0.088$) or *c-MYC* high versus low ($P = 0.14$) were not statistically significant, combined expression of *ECD* + *c-MYC* high versus *ECD* + *c-MYC* low exhibited statistically significant differences in DMFS ($P = 0.013$; Supplementary Fig. S6H). Taken together, these results suggest that combination of *c-MYC* and *ECD* gene expression may provide better prognostic value for RFS and DMFS in patients with breast cancer.

## Discussion

The evolutionarily conserved ECD protein has emerged as a key regulator of several basic cell biological processes, including the cell-cycle progression (8, 10), mRNA biogenesis (2–5), and stress responses (11), and these functional attributes together with its overexpression in human cancers and the association of such overexpression with shorter patient survival (4, 5, 14) support its potential prooncogenic function. In this study, we express an inducible *ECD* transgene in mouse mammary epithelium and demonstrate that ECD overexpression by itself promotes mammary tumorigenesis. We provide evidence that *ECD* overexpression leads to upregulation of c-MYC and its metabolic target genes, which likely mediate ECD-driven tumorigenesis.

Transgenic expression of a Tet(O)-ECD construct and crossing of these mice to a MMTV-tTA mouse (19) allowed constitutive mammary epithelium-selective overexpression of ECD in the absence of doxycycline (Supplementary Fig. S1). Mammary alveolar hyperplasia in 85% of 5 to 6 months old *ECD*Tg mice together with mammary tumor development in about a third of *ECD*Tg mice by 15 to 25 months of age, with rare lung metastasis (**Fig. 1**; Supplementary Fig. S1–S3; and Supplementary Table S1), provided support for an oncogenic function of overexpressed ECD. Mammary hyperplasia was similar to that seen with low-density lipoprotein receptor-related protein 6 (Wnt signaling co-receptor), Ron, and Six1 transgenic mice (20, 43, 44). The low metastatic potential is comparable with transgenic models of several putative oncogenic drivers, including *c-MYC*, and *WNT1* (23, 45, 46). *ECD*Tg tumors were highly heterogeneous with distinct histologic subtypes, including the squamous adenocarcinoma, papillary carcinoma, spindle cell tumor, carcinoma with fibrosis, solid carcinoma, and undifferentiated adenocarcinoma (**Fig. 1**), similar to other GEMM models (20, 21, 23, 27, 34). MMTV–c-MYC mice exhibit diverse histologic subtyped tumors including squamous carcinoma, adenosquamous carcinoma, spindle cell carcinoma (EMT), solid carcinoma, papillary, micro acinar, and mixed (23) similar to *ECD*Tg tumors. Most *ECD*Tg tumors also exhibited intratumoral heterogeneity with both squamous ($CK14^+$, $p63^+$) and epithelial ($CK18^+$) components (**Fig. 2**) and similar to other published models (21, 30, 31). Intratumoral heterogeneity has been recognized from both clinical and pathologic point of view in breast cancer and thought to be generated through subclonal evolution during tumor progression (47). Such variability within a tumor may be attributed to cancer stem cell (CSC) theory. Our initial observations indicating potential role of ECD in CSCs regulation may attribute to its display of intratumoral heterogeneity in *ECD*Tg tumors. The frequent finding of spindle-shaped morphology (30) suggested the prevalence of EMT in *ECD*Tg tumors and upregulation of vimentin, slug, and twist are consistent with this (**Fig. 2**). Of note, 41% of tumors showed $ER^+$ staining on a subset of tumor cells (**Fig. 2**) while lacking ErbB2/HER2 overexpression, similar to some reported GEMMs (31, 34).

RNA-seq analysis of *ECD*Tg tumors versus normal mammary glands identified gene expression signatures consistent with the morphology and marker-based tumor subtypes (**Fig. 4E–H**). In addition, 85% of the remaining *ECD*Tg mice exhibited preneoplastic lesions (**Fig. 1**), similar to Wap-Epimorphin mice (24). Because aging FVB mice have been reported to develop hyperplasia (25, 26), we carefully examined our control mouse cohort and found preneoplastic lesions in only 27% of control mice, with clearly distinct histology in control versus *ECD*Tg mice (Supplementary Table S2). The mammary epithelium of older FVB/N strain mice can develop rare squamous metaplasia under chronic prolactin secretion (25, 26). However, only 2 (out of 11 analyzed) of the tumor-bearing *ECD*Tg mice were parous, and hyperplastic lesions were only analyzed in nulliparous mice (Supplementary Table S1 and S2). These findings establish ECD as a genuine oncogenic driver/co-driver. We demonstrate that ECD expression is required to maintain the tumorigenic phenotype (**Fig. 3**), and tumorigenicity upon transplantation of *ECD*Tg tumor fragments into NSG mice (**Fig. 3H** and **I**; Supplementary Fig. S4; **Fig. 3J** and **K**).

Consistent with our previous findings that mammalian ECD is critical for cell-cycle entry (10), *ECD*Tg tumors exhibited high Ki-67 staining (**Fig. 2D**). RNA-seq analysis of *ECD*Tg tumors showed that genes associated with the basal subtype of breast cancer, cell cycle, and transcription were upregulated.

Upregulation of c-MYC and c-MYC target genes in tumors (**Fig. 4**) supported a potentially important role of c-MYC in mediating ECD-driven oncogenesis. Notably, a reduction in c-MYC levels upon doxycycline-induced ECD depletion in *ECD*Tg tumor organoids *in vitro* and in tumor implants *in vivo* (**Fig. 5D** and **E**) together with an increase in c-MYC mRNA and protein levels in *ECD*Tg tumors (**Fig. 5A** and **B**) suggested that ECD overexpression upregulates c-MYC levels. Doxycycline-inducible overexpression of ECD in hMECs further confirmed the ECD dependent upregulation of c-MYC (**Fig. 6**). Prevalence of EMT in *ECD*Tg tumors and their growth as organoids, indicative of an ECD-driven stemness program, are further consistent with a role of c-MYC (48).

Consistent with our previous results in mammalian systems (4, 5) and data from others using drosophila (2) which showed that ECD promotes mRNA splicing, the overexpression of ECD promoted the conversion of c-MYC pre-mRNA to mRNA (**Fig. 6I–M**) as well as c-MYC mRNA stability (**Fig. 6N** and **O**). Notably, ECD also positively regulated the c-MYC protein stability (**Fig. 6P–S**). Given ECD's interaction with the mRNA processing machinery components, its functional role in both pre-mRNA to mRNA conversion and in mRNA export (4, 5), it is likely that ECD-dependent stabilization of c-MYC mRNA reflects the more efficient processing of c-MYC mRNA into a stable, mature form. However, the possibility that ECD might regulate c-MYC mRNA transcription remains. Increased c-MYC mRNA levels likely provide a major mechanism for increased c-MYC protein levels upon ECD overexpression and vice versa. At present, ECD's positive role to regulate the c-MYC protein stability remains unexplained. We speculate that ECD may regulate c-MYC protein stability through its interaction with the R2TP cochaperone complex, which is known to promote protein folding (8). Consistent with this speculation, RUVBL1 and RUVBL2, two essential components of the R2TP complex, have been shown to interact with MYC and help stabilize it (49, 50). Taken together, our results support the idea that ECD regulates c-MYC mRNA and protein levels to potentially mediate its oncogenic function.

Human ECD gene was first cloned through complementation of growth defect in glycolytic gene transcriptional activator (GCR2)-null yeast strain lacking a key glycolytic pathway transcriptional response, known as human suppressor GCR2 (51). Since

ECD is not a transcription factor, it is reasonable to posit that ECD likely regulates cellular metabolism through a transcription factor intermediary, such as c-MYC. This hypothesis is supported by our RNA-seq analysis where *ECD*Tg tumors exhibited c-MYC metabolic gene signature, and we further confirmed by metabolomics studies showing increased glucose uptake, glycolysis, glycolytic genes expression in *ECD*Tg tumor organoids (**Fig. 7**). Opposite effects were seen upon reduction of ECD levels, with rescue by mouse ECD (human ECD siRNA resistant), or c-MYC overexpression. Taken together, these findings support a mechanistic connection of ECD-driven oncogenesis through c-MYC. Consistent with this idea, we also present evidence for a correlation between *ECD* and *c-MYC* mRNA levels across major subtypes of breast cancer (Supplementary Fig. S6A–S6F) and show that ECD and c-MYC together predict shorter RFS and DMFS in patients with breast cancer (Supplementary Fig. S6G and S6H). Interestingly, overexpression of ECD together with c-MYC predicts poorer survival in patients, indicating its regulation of other oncogenic pathways, in addition to c-MYC. ECD as a vital player in mRNA processing may regulate a variety of oncoproteins to promote oncogenesis. Secondly, being a part of R2TP complex (PAQosome complex) ECD may mediate proper protein folding of other oncoproteins, such as phosphatidylinositol-3 kinase-related protein kinase (PIKK) signaling, RNA polymerase II (RNAP II) assembly, mitotic spindle assembly, and apoptosis (52–54) to promote oncogenesis. Several members of the R2TP complex, such as RUVBL1 and RUVBL2 are known to be overexpressed in various cancers (50, 54).

In conclusion, we demonstrate that transgenic ECD overexpression targeted to mouse mammary epithelium leads to mammary ductal hyperplasia followed by the development of heterogeneous mammary tumors with transcriptional upregulation of c-MYC and its downstream metabolic target genes, supporting a novel prooncogenic role for overexpressed ECD.

## Authors' Disclosures

F. Qiu reports grants from NIH; and grants from Department of Defense during the conduct of the study. P.K. Singh reports grants from NCI outside the submitted work. H. Band reports grants from Department of Defense; and grants from NIH during the conduct of the study. V. Band reports grants from NIH; and grants from Department of Defense during the conduct of the study. No disclosures were reported by the other authors.

## Authors' Contributions

**B.C. Mohapatra:** Conceptualization, data curation, formal analysis, validation, investigation, visualization, methodology, writing–original draft. **S. Mirza:** Conceptualization, formal analysis, validation, methodology, writing–original draft. **A. Bele:** Formal analysis, methodology. **C.B. Gurumurthy:** Formal analysis, validation, methodology. **M. Raza:** Formal analysis, validation, methodology. **I. Saleem:** Formal analysis, methodology. **M.D. Storck:** Validation. **A. Sarkar:** Validation, methodology. **S.S. Kollala:** Validation, methodology. **S.K. Shukla:** Validation, methodology. **S. Southekal:** Software, validation, methodology. **K.-U. Wagner:** Resources, validation, writing–review and editing. **F. Qiu:** Software, formal analysis, writing–review and editing. **S.M. Lele:** Writing–review and editing. **M.A. Alsaleem:** Software, formal analysis. **E.A. Rakha:** Writing–review and editing. **C. Guda:** Writing–review and editing. **P.K. Singh:** Writing–review and editing. **R.D. Cardiff:** Writing–review and editing. **H. Band:** Conceptualization, resources, supervision, funding acquisition, writing–review and editing. **V. Band:** Conceptualization, resources, supervision, funding acquisition, writing–review and editing.

## Acknowledgments

This work was supported by the NIH (grant nos. R21CA241055 and R03CA253193 to V. Band); Department of Defense (grant nos. W81XWH-17–1-0616 and W81XWH-20–1-0058 to H. Band, and grant no. W81XWH-20–1-0546 to V. Band); Nebraska Initiative Grants to V. Band and S. Mirza. Support for the University of Nebraska Medical Center Genomics (Omaha, NE) was from NCI Support Grant P30CA036727 to the Fred and Pamela Buffett Cancer Center (Omaha, NE).

We thank Dr. Alexander David Borowsky (UC Davis; Davis, CA) for his valuable advice during writing of the manuscript. We would like to acknowledge the University of Nebraska Medical Center Mouse Genome Engineering, Tissue Science, Advanced Microscope, Genomics and Bioinformatics core facilities for their technical support of this work.

The costs of publication of this article were defrayed in part by the payment of page charges. This article must therefore be hereby marked *advertisement* in accordance with 18 U.S.C. Section 1734 solely to indicate this fact.

## Note

Supplementary data for this article are available at Molecular Cancer Research Online (http://mcr.aacrjournals.org/).

Received February 15, 2022; revised May 3, 2022; accepted June 3, 2022; published first June 8, 2022.

## References

1. Gaziova I, Bonnette PC, Henrich VC, Jindra M. Cell-autonomous roles of the ecdysoneless gene in Drosophila development and oogenesis. Development 2004;131:2715–25.
2. Claudius AK, Romani P, Lamkemeyer T, Jindra M, Uhlirova M. Unexpected role of the steroid-deficiency protein ecdysoneless in pre-mRNA splicing. PLoS Genet 2014;10:e1004287.
3. Erkelenz S, Stankovic D, Mundorf J, Bresser T, Claudius AK, Boehm V, et al. Ecd promotes U5 snRNP maturation and Prp8 stability. Nucleic Acids Res 2021;49:1688–707.
4. Saleem I, Mirza S, Sarkar A, Raza M, Mohapatra B, Mushtaq I, et al. The mammalian ecdysoneless protein interacts with RNA helicase DDX39A to regulate nuclear mRNA export. Mol Cell Biol 2021;41:e0010321.
5. Mirza S, Kalluchi A, Raza M, Saleem I, Mohapatra B, Pal D, et al. Ecdysoneless protein regulates viral and cellular mRNA splicing to promote cervical oncogenesis. Mol Cancer Res 2022;20:303–18.
6. Mir RA, Lovelace J, Schafer NP, Simone PD, Kellezi A, Kolar C, et al. Biophysical characterization and modeling of human Ecdysoneless (ECD) protein supports a scaffolding function. AIMS Biophys 2016;3:195–208.
7. Horejsi Z, Stach L, Flower TG, Joshi D, Flynn H, Skehel JM, et al. Phosphorylation-dependent PIH1D1 interactions define substrate specificity of the R2TP cochaperone complex. Cell Rep 2014;7:19–26.
8. Mir RA, Bele A, Mirza S, Srivastava S, Olou AA, Ammons SA, et al. A novel interaction of ecdysoneless (ECD) protein with R2TP complex component RUVBL1 is required for the functional role of ECD in cell cycle progression. Mol Cell Biol 2015;36:886–99.
9. Malinova A, Cvackova Z, Mateju D, Horejsi Z, Abeza C, Vandermoere F, et al. Assembly of the U5 snRNP component PRPF8 is controlled by the HSP90/R2TP chaperones. J Cell Biol 2017;216:1579–96.
10. Kim JH, Gurumurthy CB, Naramura M, Zhang Y, Dudley AT, Doglio L, et al. Role of mammalian Ecdysoneless in cell cycle regulation. J Biol Chem 2009;284:26402–10.
11. Olou AA, Sarkar A, Bele A, Gurumurthy CB, Mir RA, Ammons SA, et al. Mammalian ECD protein is a novel negative regulator of the PERK arm of the unfolded protein response. Mol Cell Biol 2017;37:e00030–17.
12. Zhang Y, Chen J, Gurumurthy CB, Kim J, Bhat I, Gao Q, et al. The human orthologue of Drosophila ecdysoneless protein interacts with p53 and regulates its function. Cancer Res 2006;66:7167–75.

13. Suh HW, Yun S, Song H, Jung H, Park YJ, Kim TD, et al. TXNIP interacts with hEcd to increase p53 stability and activity. Biochem Biophys Res Commun 2013; 438:264–9.
14. Zhao X, Mirza S, Alshareeda A, Zhang Y, Gurumurthy CB, Bele A, et al. Overexpression of a novel cell cycle regulator ecdysoneless in breast cancer: a marker of poor prognosis in HER2/neu-overexpressing breast cancer patients. Breast Cancer Res Treat 2012;134:171–80.
15. Dey P, Rachagani S, Chakraborty S, Singh PK, Zhao X, Gurumurthy CB, et al. Overexpression of ecdysoneless in pancreatic cancer and its role in oncogenesis by regulating glycolysis. Clin Cancer Res 2012;18:6188–98.
16. Xu SH, Zhu S, Wang Y, Huang JZ, Chen M, Wu QX, et al. ECD promotes gastric cancer metastasis by blocking E3 ligase ZFP91-mediated hnRNP F ubiquitination and degradation. Cell Death Dis 2018;9:479.
17. Bele A, Mirza S, Zhang Y, Ahmad Mir R, Lin S, Kim JH, et al. The cell cycle regulator ecdysoneless cooperates with H-Ras to promote oncogenic transformation of human mammary epithelial cells. Cell Cycle 2015;14:990–1000.
18. Shukla SK, Purohit V, Mehla K, Gunda V, Chaika NV, Vernucci E, et al. MUC1 and HIF-1alpha signaling crosstalk induces anabolic glucose metabolism to impart gemcitabine resistance to pancreatic cancer. Cancer Cell 2017;32:71–87.
19. Sakamoto K, Schmidt JW, Wagner KU. Generation of a novel MMTV-tTA transgenic mouse strain for the targeted expression of genes in the embryonic and postnatal mammary gland. PLoS One 2012;7:e43778.
20. McCoy EL, Iwanaga R, Jedlicka P, Abbey NS, Chodosh LA, Heichman KA, et al. Six1 expands the mouse mammary epithelial stem/progenitor cell pool and induces mammary tumors that undergo epithelial-mesenchymal transition. J Clin Invest 2009;119:2663–77.
21. Hollern DP, Swiatnicki MR, Andrechek ER. Histological subtypes of mouse mammary tumors reveal conserved relationships to human cancers. PLoS Genet 2018;14:e1007135.
22. Duivenvoorden HM, Spurling A, O'Toole SA, Parker BS. Discriminating the earliest stages of mammary carcinoma using myoepithelial and proliferative markers. PLoS One 2018;13:e0201370.
23. Andrechek ER, Cardiff RD, Chang JT, Gatza ML, Acharya CR, Potti A, et al. Genetic heterogeneity of Myc-induced mammary tumors reflecting diverse phenotypes including metastatic potential. Proc Natl Acad Sci U S A 2009; 106:16387–92.
24. Bascom JL, Fata JE, Hirai Y, Sternlicht MD, Bissell MJ. Epimorphin overexpression in the mouse mammary gland promotes alveolar hyperplasia and mammary adenocarcinoma. Cancer Res 2005;65:8617–21.
25. Cardiff RD, Anver MR, Gusterson BA, Hennighausen L, Jensen RA, Merino MJ, et al. The mammary pathology of genetically engineered mice: the consensus report and recommendations from the Annapolis meeting. Oncogene 2000;19: 968–88.
26. Wakefield LM, Thordarson G, Nieto AI, Shyamala G, Galvez JJ, Anver MR, et al. Spontaneous pituitary abnormalities and mammary hyperplasia in FVB/NCr mice: implications for mouse modeling. Comp Med 2003;53:424–32.
27. Jiang Z, Deng T, Jones R, Li H, Herschkowitz JI, Liu JC, et al. Rb deletion in mouse mammary progenitors induces luminal-B or basal-like/EMT tumor subtypes depending on p53 status. J Clin Invest 2010;120:3296–309.
28. Saha SK, Choi HY, Kim BW, Dayem AA, Yang GM, Kim KS, et al. KRT19 directly interacts with beta-catenin/RAC1 complex to regulate NUMB-dependent NOTCH signaling pathway and breast cancer properties. Oncogene 2017;36: 332–49.
29. Prasad ML, Huang Y, Pellegata NS, de la Chapelle A, Kloos RT. Hashimoto's thyroiditis with papillary thyroid carcinoma (PTC)-like nuclear alterations express molecular markers of PTC. Histopathology 2004;45:39–46.
30. Damonte P, Gregg JP, Borowsky AD, Keister BA, Cardiff RD. EMT tumorigenesis in the mouse mammary gland. Lab Invest 2007;87:1218–26.
31. Ponzo MG, Lesurf R, Petkiewicz S, O'Malley FP, Pinnaduwage D, Andrulis IL, et al. Met induces mammary tumors with diverse histologies and is associated with poor outcome and human basal breast cancer. Proc Natl Acad Sci U S A 2009;106:12903–8.
32. Mohibi S, Mirza S, Band H, Band V. Mouse models of estrogen receptor-positive breast cancer. J Carcinog 2011;10:35.
33. Sakamoto K, Schmidt JW, Wagner KU. Mouse models of breast cancer. Methods Mol Biol 2015;1267:47–71.
34. Graveel CR, DeGro ot JD, Su Y, Koeman J, Dykema K, Leung S, et al. Met induces diverse mammary carcinomas in mice and is associated with human basal breast cancer. Proc Natl Acad Sci U S A 2009;106:12909–14.
35. Adams JR, Xu K, Liu JC, Agamez NM, Loch AJ, Wong RG, et al. Cooperation between Pik3ca and p53 mutations in mouse mammary tumor formation. Cancer Res 2011;71:2706–17.
36. Lim E, Vaillant F, Wu D, Forrest NC, Pal B, Hart AH, et al. Aberrant luminal progenitors as the candidate target population for basal tumor development in BRCA1 mutation carriers. Nat Med 2009;15:907–13.
37. Varticovski L, Hollingshead MG, Robles AI, Wu X, Cherry J, Munroe DJ, et al. Accelerated preclinical testing using transplanted tumors from genetically engineered mouse breast cancer models. Clin Cancer Res 2007;13: 2168–77.
38. Malvia S, Bagadi SAR, Pradhan D, Chintamani C, Bhatnagar A, Arora D, et al. Study of gene expression profiles of breast cancers in Indian women. Sci Rep 2019;9:10018.
39. Bild AH, Yao G, Chang JT, Wang Q, Potti A, Chasse D, et al. Oncogenic pathway signatures in human cancers as a guide to targeted therapies. Nature 2006;439: 353–7.
40. Kim JW, Gao P, Liu YC, Semenza GL, Dang CV. Hypoxia-inducible factor 1 and dysregulated c-Myc cooperatively induce vascular endothelial growth factor and metabolic switches hexokinase 2 and pyruvate dehydrogenase kinase 1. Mol Cell Biol 2007;27:7381–93.
41. Miller DM, Thomas SD, Islam A, Muench D, Sedoris K. c-Myc and cancer metabolism. Clin Cancer Res 2012;18:5546–53.
42. Gyorffy B, Lanczky A, Eklund AC, Denkert C, Budczies J, Li Q, et al. An online survival analysis tool to rapidly assess the effect of 22,277 genes on breast cancer prognosis using microarray data of 1,809 patients. Breast Cancer Res Treat 2010; 123:725–31.
43. Zhang J, Li Y, Liu Q, Lu W, Bu G. Wnt signaling activation and mammary gland hyperplasia in MMTV-LRP6 transgenic mice: implication for breast cancer tumorigenesis. Oncogene 2010;29:539–49.
44. Zinser GM, Leonis MA, Toney K, Pathrose P, Thobe M, Kader SA, et al. Mammary-specific Ron receptor overexpression induces highly metastatic mammary tumors associated with beta-catenin activation. Cancer Res 2006; 66:11967–74.
45. Li Y, Hively WP, Varmus HE. Use of MMTV-Wnt-1 transgenic mice for studying the genetic basis of breast cancer. Oncogene 2000;19:1002–9.
46. Mori H, Cardiff RD, Borowsky AD. Aging mouse models reveal complex tumor-microenvironment interactions in cancer progression. Front Cell Dev Biol 2018; 6:35.
47. Almendro V, Marusyk A, Polyak K. Cellular heterogeneity and molecular evolution in cancer. Annu Rev Pathol 2013;8:277–302.
48. Kim J, Woo AJ, Chu J, Snow JW, Fujiwara Y, Kim CG, et al. A Myc network accounts for similarities between embryonic stem and cancer cell transcription programs. Cell 2010;143:313–24.
49. Wood MA, McMahon SB, Cole MD. An ATPase/helicase complex is an essential cofactor for oncogenic transformation by c-Myc. Mol Cell 2000;5:321–30.
50. Zhang X, Ren J, Yan L, Tang Y, Zhang W, Li D, et al. Cytoplasmic expression of pontin in renal cell carcinoma correlates with tumor invasion, metastasis and patients' survival. PLoS One 2015;10:e0118659.
51. Sato T, Jigami Y, Suzuki T, Uemura H. A human gene, hSGT1, can substitute for GCR2, which encodes a general regulatory factor of glycolytic gene expression in Saccharomyces cerevisiae. Mol Gen Genet 1999;260:535–40.
52. Boulon S, Bertrand E., Pradet-Balade B. HSP90 and the R2TP co-chaperone complex: building multi-protein machineries essential for cell growth and gene expression. RNA Biol 2012;9:148–54.
53. Lynham J, Houry WA. The multiple functions of the PAQosome: An R2TP- and URI1 prefoldin-based chaperone complex. Adv Exp Med Biol 2018;1106: 37–72.
54. Mao YQ, Houry WA. The role of pontin and reptin in cellular physiology and cancer etiology. Front Mol Biosci 2017;4:58.